*Am J Physiol Heart Circ Physiol* 286: H1836–H1844, 2004.
First published January 2, 2004; 10.1152/ajpheart.00123.2003.

# Intracellular Ca dynamics in ventricular fibrillation

**Chikaya Omichi, Scott T. Lamp, Shien-Fong Lin, Junzhong Yang, Ali Baher, Shengmei Zhou, Mina Attin, Moon-Hyoung Lee, Hrayr S. Karagueuzian, Boris Kogan, Zhilin Qu, Alan Garfinkel, Peng-Sheng Chen, and James N. Weiss**

*Division of Cardiology, Cedars-Sinai Medical Center and Center for Health Sciences, University of California-Los Angeles (UCLA) Cardiovascular Research Laboratory, Departments of Medicine, Physiology, Physiological Science, and Computer Science, David Geffen School of Medicine, UCLA, Los Angeles, California 90095*

Submitted 13 February 2003; accepted in final form 16 December 2003

**Omichi, Chikaya, Scott T. Lamp, Shien-Fong Lin, Junzhong Yang, Ali Baher, Shengmei Zhou, Mina Attin, Moon-Hyoung Lee, Hrayr S. Karagueuzian, Boris Kogan, Zhilin Qu, Alan Garfinkel, Peng-Sheng Chen, and James N. Weiss.** Intracellular Ca dynamics in ventricular fibrillation. *Am J Physiol Heart Circ Physiol* 286: H1836–H1844, 2004. First published January 2, 2004; 10.1152/ajpheart.00123.2003.—In the heart, membrane voltage ($V_m$) and intracellular Ca ($Ca_i$) are bidirectionally coupled, so that ionic membrane currents regulate $Ca_i$ cycling and $Ca_i$ affects ionic currents regulating action potential duration (APD). Although $Ca_i$ reliably and consistently tracks $V_m$ at normal heart rates, it is possible that at very rapid rates, sarcoplasmic reticulum $Ca_i$ cycling may exhibit intrinsic dynamics. Non-voltage-gated $Ca_i$ release might cause local alternations in APD and refractoriness that influence wavebreak during ventricular fibrillation (VF). In this study, we tested this hypothesis by examining the extent to which $Ca_i$ is associated with $V_m$ during VF. $Ca_i$ transients were mapped optically in isolated arterially perfused swine right ventricles using the fluorescent dye rhod 2 AM while intracellular membrane potential was simultaneously recorded either locally with a microelectrode (5 preparations) or globally with the voltage-sensitive dye RH-237 (5 preparations). Mutual information (MI) is a quantitative statistical measure of the extent to which knowledge of one variable ($V_m$) predicts the value of a second variable ($Ca_i$). MI was high during pacing and ventricular tachycardia (VT; $1.13 \pm 0.21$ and $1.69 \pm 0.18$, respectively) but fell dramatically during VF ($0.28 \pm 0.06$, $P < 0.001$). $Ca_i$ at sites 4–6 mm apart also showed decreased MI during VF ($0.63 \pm 0.13$) compared with pacing ($1.59 \pm 0.34$, $P < 0.001$) or VT ($2.05 \pm 0.67$, $P < 0.001$). Spatially, $Ca_i$ waves usually bore no relationship to membrane depolarization waves during nonreentrant fractionated waves typical of VF, whereas they tracked each other closely during pacing and VT. The dominant frequencies of $V_m$ and $Ca_i$ signals analyzed by fast Fourier transform were similar during VT but differed significantly during VF. $Ca_i$ is closely associated with $V_m$ closely during pacing and VT but not during VF. These findings suggest that during VF, non-voltage-gated $Ca_i$ release events occur and may influence wavebreak by altering $V_m$ and APD locally.

calcium transient; action potential; cardiac restitution; optical mapping

IT IS WELL KNOWN that the intracellular Ca ($Ca_i$) transient shapes cardiac action potential (AP) characteristics by modulating Ca-sensitive ionic currents, such as the L-type Ca channel, Na-Ca exchange, and Ca-activated Cl and nonselective channels (26). $Ca_i$ overload also predisposes the myocardium to delayed and early afterdepolarizations, which may contribute to the initiation and perpetuation of cardiac arrhythmias. During ventricular fibrillation (VF), diastolic $Ca_i$ may increase to systolic levels (24), potentially triggering spontaneous (i.e., nonvoltage triggered) Ca release from the sarcoplasmic reticulum (SR). This raises the possibility that VF may be maintained in part by effects of Ca-sensitive membrane currents on AP propagation (13). Previously, we reported that in simulated cardiac tissue, spiral waves could be destabilized and induced to breakup into a fibrillation-like state as a result of spontaneously developing spatial nonuniformities in $Ca_i$ caused by spontaneous Ca-induced Ca release (4). If spontaneous Ca-induced Ca release was prevented, the spiral wave remained intact and did not break up. In this same study, we also demonstrated experimentally that $Ca_i$ release in isolated cardiac myocytes exhibited intrinsic complex dynamics independent of membrane voltage ($V_m$). When isolated myocytes were paced at rapid rates under AP clamp conditions (so that $V_m$ had a fixed waveform), beat-to-beat $Ca_i$ release developed alternans and more complex periodicities, indicating that Ca-induced Ca release was being regulated by other factors besides $V_m$ alone. We speculated that during VF, the interaction between $Ca_i$-release dynamics and AP dynamics might influence, and perhaps enhance, wavebreak in intact cardiac tissue.

Direct assessment of the role of $Ca_i$ dynamics in wave stability during VF in intact tissue is difficult because $V_m$ and $Ca_i$ cycling are highly interdependent and bidirectionally coupled. It is not possible in intact tissue to control one process (i.e., by voltage or $Ca_i$ clamp) to study the other. This limitation necessitates indirect approaches. A first step in understanding whether the two processes may destabilize each other is to determine whether $Ca_i$ cycling is reliably and consistently associated with $V_m$ during VF. If so, then it is less likely that non-voltage-gated $Ca_i$ release occurs and that $Ca_i$ dynamics contribute independently to wavebreak during VF. The purpose of this study was to test this hypothesis by comparing how closely $Ca_i$ and $V_m$ are associated with each other in arterially perfused swine right ventricles (RVs) during VF compared with pacing and ventricular tachycardia (VT).

## METHODS

The research protocol was approved by the Institutional Animal Care and Use Committee and followed the guidelines of the American Heart Association.

*Tissue preparation.* Eleven farm pigs (weighing 25–32 kg) of either sex were anesthetized with 20 mg/kg iv thiopental sodium. The chest was opened with a median sternotomy, the hearts were removed,

Address for reprint requests and other correspondence: J. N. Weiss, Rm. 3645, MRL Bldg., Cardiovascular Research Laboratory, David Geffen School of Medicine, UCLA, Los Angeles, CA 90095-1760 (E-mail: jweiss@mednet.ucla.edu).

The costs of publication of this article were defrayed in part by the payment of page charges. The article must therefore be hereby marked "*advertisement*" in accordance with 18 U.S.C. Section 1734 solely to indicate this fact.

  

and the RV was perfused through the right coronary artery as described previously (10). The isolated RV was placed with the endocardial side up in a tissue bath. In addition to continuous arterial perfusion, the entire tissue was also superfused with 37°C oxygenated Tyrode solution at a flow rate of 20 ml/min. The composition of the solution was as follows (in mmol/l): 125.0 NaCl, 4.5 KCl, 0.5 $MgCl_2$, 0.54 $CaCl_2$, 1.2 $NaH_2PO_4$, 24.0 $NaHCO_3$, and 5.5 glucose with 50 mg/l albumin; pH 7.35. Extracellular [Ca] was reduced to decrease motion artifacts because no excitation-contraction uncouplers were used to suppress contraction. Bipolar electrodes, a pacing electrode, and pseudo-ECG electrodes were attached to the endocardial surface. A pair of defibrillation coil electrodes (Guidant) were placed on either side of the tissue bath and were connected to a HVS-02 external defibrillator (Ventritex).

In all isolated RV tissues, spontaneous VT or VF occurred during the isolation procedure (presumably induced by the combination of transient ischemia and mechanical manipulation) and persisted with stable characteristics after arterial perfusion was achieved unless defibrillated. $Ca_i$ transients during VT and VF were mapped while $V_m$ was simultaneously recorded either optically or with microelectrodes. Biphasic shocks of 1.5–3.0 J were used to defibrillate the RV. The RV was then paced with electrical stimuli of 2-ms duration and twice diastolic threshold current at 400 ms.

*Transmembrane AP recording.* In five preparations, $V_m$ was recorded with a standard glass microelectrode filled with 3 mol/l KCl and digitized at 3.13 kHz with 12-bit accuracy (Axon Instruments). The microelectrode was coupled with an Ag-AgCl wire leading to amplifiers with a high input impedance and variable-capacity neutralization (Am-2 and ME-3221, Warner Instruments). Microelectrode impalements were made in a region injected with the fluorescent Ca indicator rhod 2 AM to measure the $Ca_i$ transient. $Ca_i$ was recorded optically using a charge-coupled device (CCD) camera as described in the next section.

*Optical mapping of $Ca_i$ and voltage.* In addition to the five preparations locally injected with rhod 2 AM, an additional five isolated, perfused swine RVs were double stained with the voltage-sensitive dye RH-237 in addition to rhod 2 AM by arterial perfusion. The double-stained heart was excited with a solid-state laser (532 nm, Verdi, Cohereht), and $V_m$ and $Ca_i$ fluorescence were recorded optically by separate CCD cameras (CA-D1-0128T, Dalsa, Ontario, Canada) using a 690-nm long-pass filter for RH-237 and a 585 ± 20-nm filter for rhod 2. The two CCD cameras were carefully aligned to image the same region. To calibrate the alignment, we placed a reference grid in the optical field to provide fiduciary points, which were used to calculate the correct positions after stretching and rotational corrections. After realignment, we ascertained the positional accuracy between the two camera images to be ±1 mm. Data were acquired at an acquisition rate of 2.3 ms/frame (435 frames/s). Spatial resolution was 128 × 128 pixels over 30 × 30 $mm^2$, corresponding to 0.25 $mm^2$ tissue/pixel.

After acquisition, fluorescence signals were baseline subtracted. The RH-237 signal was inverted to show increased $V_m$ in the upward direction. A moving median temporal filter of 5 data points (sampled at 2.3 ms/point) was applied, after which the signals at each pixel were normalized on a scale from 0 to 256 (with the average of the lowest 5 values assigned 0 and the average of the 5 maximal values assigned 256). The signal at each pixel was then spatially averaged with the signals of eight neighboring pixels to improve the signal-to-noise ratio. The overall recording area after spatial filtering was therefore estimated at 0.75 $mm^2$, with a 1-mm uncertainty between the relative positions of the $V_m$ and $Ca_i$ recording sites as noted above. Data were displayed using MATLAB (Math Works; Natick, MA), ORIGIN (Microcal Software; Northampton, MA), and customized (Wavefinder) software. In spatial maps, both $V_m$ and $Ca_i$ were color coded from red (highest voltage) to blue (lowest). Wavelets were identified using our previously described depolarization wavefront and repolarization waveback detection algorithm (11). Points in which depolarization and repolarization met were defined as wavebreak points. Reentry was defined as wavefront rotation around a wavebreak point completing a 360° cycle (although a stationary center of rotation was not required).

The level of cross-talk between the optically measured voltage and Ca dyes was assessed by staining preparations with only one dye and then measuring the optical signals at both wavelengths from the dual CCD cameras (Fig. 1). The absolute level of fluorescence detected in the Ca channel when the preparation was stained with RH-237 but not rhod 2 averaged <1% of the signal compared with when rhod 2 was present. Modulation of the $Ca_i$ signal (i.e., the difference between maximum and minimum levels of fluorescence at each pixel) under these conditions was also <1% of the modulation in the voltage channel (Fig. 1). Conversely, with rhod 2 present but no RH-237 staining, the signal averaged <1% of the signal when RH-237 was

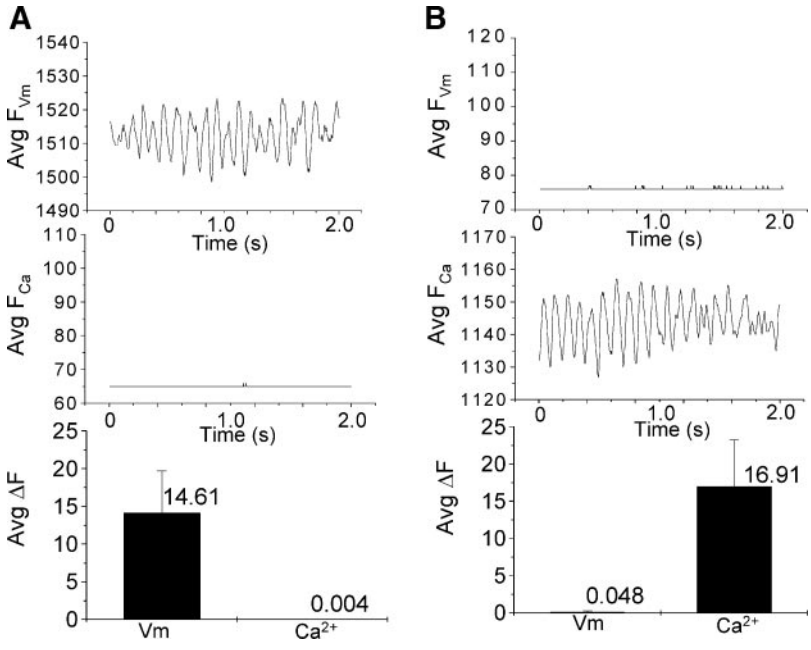


Fig. 1. Lack of cross-talk between optical dye signals for membrane voltage ($V_m$) and intacellular Ca ($Ca_i$). *A*: average (Avg) fluorescence value at all pixels for simultaneously recorded signals from the $V_m$ channel ($F_{V_m}$; RH-237, *top*) and the Ca channel ($F_{Ca}$; rhod 2, *middle*) during ventricular fibrillation (VF) in a porcine right ventricle (RV) stained only with RH-237. *Bottom*, average value of the difference between the maximum and minimum fluorescence value (ΔF) at each pixel for both channels. *B*: equivalent data for a porcine RV stained only with rhod 2 AM.

present. Thus cross-talk between the optical voltage and $Ca_i$ signals was insignificant.

*Computer modeling.* We carried out computer simulations in a two-dimensional (2-D) tissue model using the following differential equation with a no-flux boundary for transmembrane voltage ($V$)

$$\frac{\partial V}{\partial t} = -I_{ion}/C_m + D\left(\frac{\partial^2 V}{\partial x^2} + \frac{\partial^2 V}{\partial y^2}\right) \quad (1)$$

where $t$ is time, $C_m$ is membrane capacitance, $D$ is the isotropic diffusion coefficient, and $x$ and $y$ are spatial coordinates. The ionic currents ($I_{ion}$) in the above equation were taken from two different AP models. First, we used the ventricular AP model developed by Fox et al. (8), in which we increased the maximum conductance of L-type Ca current by 50% to produce sustained spiral wave break up. In this model, the Ca transient is passively triggered by voltage. Second, we used the same modifications to the Fox et al. model but substituted a new formulation of $Ca_i$ cycling developed by us. In this new model, Ca cyclng is dynamically active by itself and oscillates independently of voltage in certain parameter regimes. The equations are as follows

$$\frac{dCa}{dt} = I_{rel} + I_{leak} - I_{up} - \left(\frac{A_{Cap}Cs}{2FV_{myo}}\right)(I_{LCa} + I_{Cab} + I_{pCa} - 2I_{NaCa}) \quad (2a)$$

$$\frac{dCa_{SR}}{dt} = -\left(\frac{A_{Cap}Cs}{2FV_{myo}}\right)(I_{LCa} + I_{Cab} + I_{pCa} - 2I_{NaCa}) \quad (2b)$$

$$\frac{dw}{dt} = \frac{(w_\infty - w)}{\tau_w} \quad (2c)$$

$$w_\infty = \frac{1}{1 + k_2^2 Ca^2} \quad (2d)$$

$$\tau_w = \frac{w_\infty Ca k_2}{k_{off}} \quad (2e)$$

$$I_{rel} = \frac{v_1 w Ca^2}{Ca^2 + k_{up}^2}(Cs - Ca) \quad (2f)$$

$$Cs = \frac{(Ca_{SR} - Ca)}{\beta} \quad (2g)$$

$$I_{leak} = v_2(Cs - Ca) \quad (2h)$$

$$I_{up} = \frac{v_{up} Ca^2}{Ca^2 + k_{up}^2} \quad (2i)$$

where Ca is the Ca concentration in the myoplasm, $I_{rel}$ is SR Ca release current, $I_{leak}$ is SR Ca leak current, $I_{up}$ is SR Ca uptake current, $A_{Cap}$ is capacitive membrane area, $F$ is Faraday's constant, $V_{myo}$ is myocardial volume, $I_{LCa}$ is L-type Ca current, $I_{Cab}$ is Ca background current, $I_{pCa}$ is SR Ca pump current, $I_{NaCa}$ is Na/Ca exchange current, $Ca_{SR}$ is the Ca concentration in the SR, $w$ is the inactivation gate variable of the SR Ca release channel, $w_\infty$ is the steady state of $w$, $\tau_w$ is the time constant for the $w$ gate, $k_2$ is a rate constant for the $w$ gate and equals 4 $mmol^{-1}$, $k_{off}$ is a rate constant for the $w$ gate and equals 0.0105 $ms^{-1}$, $v_1$ is the maximum conductance of $I_{rel}$ and equals 0.02, $k_{up}$ is a rate constant for the activation gate of $I_{rel}$ and equals 0.25 mmol, $\beta$ is a constant for the volume factor and equals 0.02, $v_2$ is the maximum conductance of $I_{leak}$ and equals $1.5 \times 10^{-4}$ $ms^{-1}$, and $v_{up}$ is the maximum conductance of $I_{up}$ and equals 0.1 $ms^{-1}$.

*Data analysis.* All data are presented as means ± SE. In the five hearts locally injected with rhod 2 AM, mutual information (MI) was used to assess the statistical dependency of $Ca_i$ on $V_m$. MI is a nonlinear measure of the statistical dependence between two variables ($x_i$ and $y_i$) that quantifies how much knowing the value of $x_i$ reduces our uncertainty in the value of $y_i$ (1). MI is a useful measure of the nonlinear relationship between two variables and is more sensitive than correlation, which can only find linear relationships. Given a voltage signal $V$ and a synchronous calcium signal Ca, we decimated the signals by first estimating the time it takes for the autocorrelation function of the signal to drop to zero. We then resampled the signal at an interval slightly greater than this "autocorrelation time," thus generating statistically independent points. MI, like most measures, requires such statistically independent data points. Given a resampled time series $V_n$ and a synchronous calcium signal $Ca_n$ ($n = 1, \ldots, N$), we formed the scatterplot $\{(V_n, Ca_n)\}$, coarse grained into a $K \times K$ grid, with columns $C_1, \ldots, C_K$ and rows $R_1, \ldots, R_K$. The basic idea is that the probability of a point falling in a box $B_{ij}$ is equal to the product of its falling in row $R_i$ times the probability of its falling in column $C_j$, provided that rows and columns are independent. MI uses the discrepancy between the two as a measure of the nonindependence of row and column, i.e., voltage and calcium. The definition is as follows: let $\#R_i$ be the number of points in row $R_i$, $\#C_j$ the number of points in column $C_j$, and $\#B_{ij}$ the number of points in box $B_{ij}$. We then define the probabilities as $P(R_i) = \#R_i/N$, $P(C_j) = \#C_j/N$, and $P(B_{ij}) = \#(B_{ij})/N$. MI is then defined as follows

$$MI = \sum_{i,j=1}^{K} P(B_{ij}) \times \log_2 P\left[\frac{P(B_{ij})}{P(R_i)P(C_j)}\right] \quad (3)$$

For our case, this results in

$$MI_{V,Ca_i} = \sum_{V_m(t_j),Ca_i(t_j)} P_{V_m,Ca_i}[V_m(t_j), Ca_i(t_j)] \log \frac{P_{V_m,Ca_i}[V_m(t_j), Ca_i(t_j)]}{P_{V_m}[V_m(t_j)]P_{Ca_i}[Ca_i(t_j)]} \quad (4)$$

where $P_{V,Ca_i}[V_m(t_j),Ca_i(t_j)]$ is the joint probability density for $V_m$ and $Ca_i$ resulting from values $V_m(t_j)$ and $Ca_i(t_j)$. $P_{V_m}[V_m(t_j)]$ and $P_{Ca_i}[Ca_i(t_j)]$ are the individual probability densities for $V_m$ and $Ca_i$. The probability densities are calculated from the data as above. Because a time lag between two variables can affect MI, we calculated MI using a range of lag times ($\tau$) from 0 to 225 ms [which exceeds the average cycle length (CL) during VT and VF]. We report the MI data by indicating the mean MI value as well as the minimum and maximum MI values over the full range of $\tau$.

The statistical significance of differences in MI among pacing, VT, and VF was assessed from the mean MI values by Student's $t$-test using the Bonferoni correction for multiple comparisons. In addition, to assess whether MI values were significantly different from randomness, we used a bootstrapping method (6) in which the mean MI for actual data was compared with the MI obtained after reshuffling the $x_i$ time series ($V_m$) and calculating MI for the reshuffled $x$ values and the original $y$ values ($Ca_i$). This procedure was iterated 100 times, and if the actual MI exceeded 95 of 100 of the MIs for the randomized time series, the MI was considered to be significant at the $P < 0.05$ level, independent of assumptions about probability distributions. MI between $V_m$ and $Ca_i$ was calculated for Ca signals recorded both near (<1 mm) and far (4–6 mm) from the microelectrode $V_m$ recording site. MI between the two $Ca_i$ signals at the near and far sites was also calculated to assess the spatial dependence of $Ca_i$ during pacing, VT, and VF.

Fast Fourier transform (FFT) spectra were derived from optical recordings as described elsewhere (25), with the dominant frequency defined as the highest peak in the 3- to 20-Hz range of the FFT spectrum. FFT spectra were determined from a recording duration of 2.3 s in all cases. Wavebreak points in voltage maps from real and simulated tissue were detected using customized software (16).

## RESULTS

*Relationships between local $Ca_i$ and local $V_m$.* Figure 2, *A–C*, shows $V_m$ (black traces) and $Ca_i$ transients from a heart loaded with rhod 2 AM by local injection during pacing (400-ms CL), VT, and VF, respectively. $Ca_i$ was recorded both near (within 1 mm, red traces) and far (4–6 mm, blue traces) from the microelectrode $V_m$ recording site. The superimposed

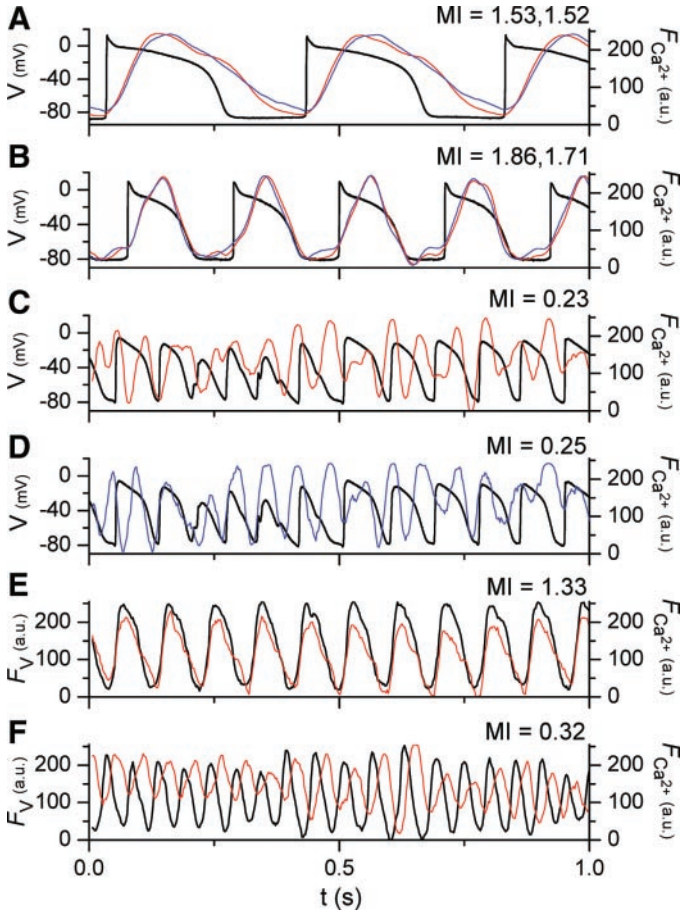


Fig. 2. The $Ca_i$ transient remains synchronized to $V_m$ during pacing and ventricular tachycardia (VT) but not during VF. *A–C*: superimposed simultaneous recordings of microelectrode $V_m$ (*V*; black traces) and optical Ca signals [$F_{Ca}$; in arbitrary units (au)] near to (<1 mm, red traces) and distant from (4–6 mm, blue traces) the microelectrode $V_m$ recording site during pacing at a cycle length of 400 ms (*A*), VT (*B*), and VF (*C* and *D*). Mutual information (MI) between $V_m$ and $F_{Ca}$ at the near and far sites are shown. *E* and *F*: representative simultaneous optical recordings of $V_m$ ($F_V$; black traces) and Ca ($F_{Ca}$; red traces) during VT (*E*) and VF (*F*) in preparations dually stained with RH-237 and rhod 2 AM. MI values are also shown. *t*, Time.

traces illustrate that $Ca_i$ is closely associated with $V_m$ closely during pacing and VT but not during the majority of VF, although brief periods of synchrony were observed. During VF, not only did $Ca_i$ fail to track $V_m$, but nearby $Ca_i$ signals also did not track each other closely. To quantify statistically how closely $Ca_i$ at near and far sites tracked $V_m$, MI was calculated as described in METHODS. Figure 3*A* shows the value of MI for simultaneous recordings of $V_m$ and $Ca_i$ during pacing, VT, and VF ($n = 5$ in each group) plotted against lag time $\tau$ (because MI is sensitive to the phase delay between the $V_m$ and $Ca_i$ traces). Figure 3*B* summarizes the mean value of MI for each experiment, with the minimum and maximum values indicated by the vertical bars. MI between $V_m$ and $Ca_i$ was much higher during pacing or VT than during VF, at both the near and far $Ca_i$ recording sites. MI was also significantly higher during VT compared with pacing because of the longer diastolic interval during pacing. This reflects the fact that $V_m$ and $Ca_i$ have a greater influence on each other during systole than during diastole. During diastole, the decay of the $Ca_i$ transient is primarily regulated by SR Ca uptake, which is independent of $V_m$. Conversely, $Ca_i$ has only a minor effect on $V_m$ because $V_m$ is dominated by the large inward rectifier K conductance, against which $Ca_i$-sensitive currents such as Na-Ca exchange have only minor influence. Because the same relatively stable value of diastolic $V_m$ is associated with many values of $Ca_i$ as the $Ca_i$ transient trails off, MI is low during diastole, decreasing the overall value of MI during the full cardiac cycle. This point reflects the robustness of MI as a sensitive quantitative measure of the extent to which $Ca_i$ and $V_m$ are associated. Moreover, this point emphasizes that the decrease in MI during VF is highly significant, because diastole is even shorter during VF, which would tend to increase MI if $Ca_i$ were passively driven by $V_m$.

To assess the degree to which MI between $V_m$ and $Ca_i$ was significant, MI for actual data was compared with MI obtained after reshuffling the $V_m$ time series and calculating MI for the reshuffled $V_m$ values and the original $Ca_i$ values. This procedure is expected to destroy any MI that exists between the $V_m$ and $Ca_i$ signals and was iterated 100 times for each episode of pacing, VT, or VF. For each pacing and VT episode, the actual MI value was greater than the 100th percentile of all 100 shuffled MI values for both the near and far $Ca_i$ recording sites. This indicates that shuffling destroyed, at the $P < 0.01$ level, the MI between $V_m$ and $Ca_i$. In contrast, for VF, the actual MI between $V_m$ and near $Ca_i$ sites fell at the 26th, 45th, 55th, 86th, and 97th percentile of the 100 shuffled MI values for 5 episodes of VF and between the 14th, 22nd, 52nd, 61st, and 91st percentile with respect to the far $Ca_i$ site. Thus the MI of the real data during VF was not statistically different (at the $P > 0.05$ level) from the randomly shuffled data in all but 9 of 10 cases. This suggests that the bidirectional influence of $V_m$ on $Ca_i$ and $Ca_i$ on $V_m$ becomes highly interactive and complex during VF, consistent with the idea that non-voltage-gated $Ca_i$ release occurs and has a strong influence on local $V_m$, which affects wave propagation.

Figure 3*C* addresses the spatial coupling of $Ca_i$ during pacing, VT, and VF by calculating MI between $Ca_i$ recorded at the near (<1 mm) and far (4–6 mm) sites. MI was high during pacing and VT but decreased significantly during VF ($P < 0.0001$). To estimate the spatial range over which MI decreased during VF, we compared MI among three sites that were <1 mm apart (near), 2–3 mm apart (intermediate), or 4–6 mm (far) (Fig. 3*C*). For five VF episodes, the mean MI between $Ca_i$ traces averaged $0.25 \pm 0.01$ for adjacent sites, $0.25 \pm 0.01$ for intermediate sites, and $0.26 \pm 0.01$ for far sites. Note that even for nearby sites, MI between Ca traces was significantly lower than that during either pacing or VT.

Five additional preparations were dually loaded with RH-237 and rhod 2 AM via the arterial perfusate to permit simultaneous optical mapping of $V_m$ and $Ca_i$ during episodes of pacing, VT, and VF. Figure 2, *E* and *F*, shows representative simultaneous optically recorded $V_m$ and $Ca_i$ traces from the same site during VT and VF, respectively. Similar to preparations in which $V_m$ was recorded with microelectrodes (Fig. 2, *B–D*), $Ca_i$ was closely associated with $V_m$ during VT (Fig. 2*E*) but not VF (Fig. 2*F*). Even though in the latter example peak $Ca_i$ appears to follow peak $V_m$ during VF, MI was much lower than during VT. It is unlikely that the $Ca_i$ signal during VF represented amplified noise, because the absolute values of fluorescence of the $Ca_i$ signal before any signal processing, as well as the difference between the minimal and maximal

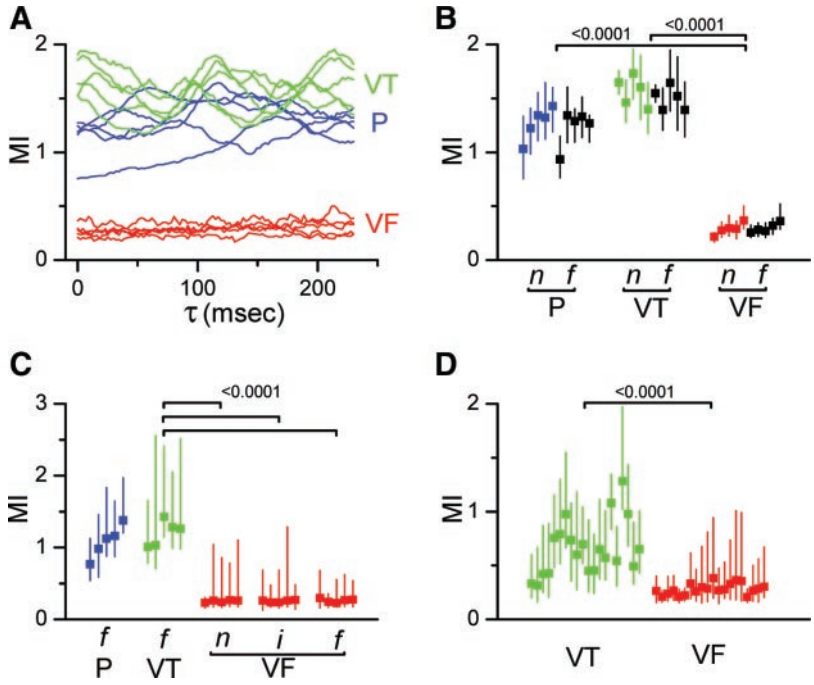


Fig. 3. MI between $V_m$ and $Ca_i$ (*A*, *B*, and *D*) and between $Ca_i$ at different sites (*C*). *A*: MI between $V_m$ and $Ca_i$ ($F_{Ca}$) during pacing (P) at 400 ms, VT (green lines), and VF (red lines) for 5 preparations in each group as a function of the time lag ($\tau$) between the $V_m$ and $Ca_i$ traces. $V_m$ was measured with a microelectrode, and $Ca_i$ was measured optically within 1 mm of the microelectrode. *B*: summary of MI values between $V_m$ and $F_{Ca}$ in *A* during pacing (blue), VT (green), and VF (red). For all values of $\tau$, the mean values of MI are indicated by the squares and the minimal and maximal MI values by the vertical lines. The black points indicate MI between $V_m$ and $F_{Ca}$ recorded far (f; 4–6 mm) from the microelectrode. *C*: mean, minimum, and maximum MI between $F_{Ca}$ at far sites 4–6 mm apart during pacing, VT, and VF. For VF, MI between $F_{Ca}$ at near sites (n; <1 mm apart) and intermediate sites (i; 2–3 mm apart) is also shown. *D*: mean, minimum, and maximum MI between $F_V$ and $F_{Ca}$ at the same sites during VT and VF in preparations dually stained with RH-237 and rhod 2 AM. *P* values comparing the mean MI values are indicated.

values, were similar during VT and VF episodes. To calculate MI between $V_m$ and $Ca_i$, four sites with good signals were selected from each quadrant of the mapped area in five episodes of VT and five episodes of VF (Fig. 3*D*). The mean MI between $V_m$ and $Ca_i$ averaged 0.66 ± 0.06 (range 0.31–1.28) during VT episodes and decreased to 0.28 ± 0.01 (range 0.21–0.38) during VF. Despite the wide variation in MI at different sites during VT evident in Fig. 3*D*, the differences between MI in VT and VF were highly significant using either the mean, maximum, or minimum values of MI ($P < 0.0001$ for all 3 cases). These findings are consistent with the experiments in which $V_m$ was measured using a microelectrode. The lower average MI value during VT when $V_m$ was recorded optically may be related to the lower signal-to-noise ratio or spatial averaging of the optical signal compared with the microelectrode $V_m$ signal.

Finally, to confirm that non-voltage-gated $Ca_i$ dynamics could account for the decrease in MI during VF, we performed simulations in 2-D homogeneous cardiac tissue using two different AP models. In one model, the $Ca_i$ transient was exclusively triggered by $V_m$ depolarization. In the other model, $Ca_i$ cycling was dynamically active on its own in addition to being triggered by voltage (see METHODS). Parameters were set to the spiral wave breakup regime in both models, characterized by multiple meandering wavelets resembling VF (Fig. 4, *A* and *B*). The means ± SD of CL (168 ± 70 vs. 190 ± 93 ms), AP duration (123 ± 50 vs. 133 ± 41 ms), and diastolic interval (49 ± 56 vs. 50 ± 60 ms) were similar during simulated VF for the passive and active $Ca_i$ cycling cases, respectively. Figure 4, *C* and *D*, shows representative traces of $V_m$ and $Ca_i$ at the same site, with $Ca_i$ passively tracking $V_m$ in the passive Ca cycling model (Fig. 4*C*) and $Ca_i$ in a self-oscillatory regime in the dynamic $Ca_i$ cycling model (Fig. 4*D*). Note the similarity of the traces in the latter case to the experimental recordings in Fig. 2*C*. Figure 4*E* shows the calculated MI between $V_m$ and $Ca_i$ as a function of $\tau$ between the $V_m$ and $Ca_i$ traces. When $Ca_i$ passively tracked $V_m$, MI during VF was high (~1.5), but when $Ca_i$ and $V_m$ were both dynamically active, MI decreased to a much lower value (~0.5), similar to values measured during experimental VF. Moreover, the incidence of wavebreak increased significantly when $Ca_i$ cycling was dynamically active, from 3.85 ± 1.89 to 7.23 ± 2.35 wavebreaks/frame ($P < 0.01$). Thus localized non-voltage-gated Ca release promoted wavebreak during simulated VF in this model.

*Relationship of $Ca_i$ waves to membrane depolarization waves.* In the five preparations dually loaded with RH-237 and rhod 2 AM, simultaneous high-resolution spatiotemporal optical mapping of $V_m$ and $Ca_i$ was performed during episodes of pacing (3 hearts), VT (3 hearts), and VF (3 hearts). During pacing (not shown) and VT (Fig. 5), $Ca_i$ waves closely tracked the spread of membrane depolarization after a delay averaging 32 ± 20 ms. During the majority of VF when multiple fractionated wavefronts were present in the mapped area, $Ca_i$ waves bore no consistent relationship to voltage waves (Fig. 6*A*). For example, at 0 ms, membrane depolarization was propagating in the upper right corner into a region in which $Ca_i$ was already elevated, as though the membrane depolarization had been preceded by Ca release. Similar findings were observed in 15 nonreentrant waves during VF in 3 hearts. Similar non-voltage-gated Ca-release events were also observed in simulated VF when $Ca_i$ cycling in the cell AP model was in a self-oscillatory mode (Fig. 4*B*, yellow oval) but not when $Ca_i$ cycling was passively driven by $V_m$ (Fig. 4*A*). Occasionally, however, cycles of complete reentry (360° loop) were observed during VF [~15% of all wavefronts (25)]. In these cases, the $Ca_i$ wave tracked the membrane depolarization wave after a brief time delay, similar to pacing and VT. Figure 6*B* shows an example in which the membrane depolarization wave had a center of rotation in the lower right corner and rotated clockwise. The $Ca_i$ wave showed an identical pattern but delayed (at 0 ms, the membrane depolarization wave is vertical at 12 o'clock and the Ca wave is at 10 o'clock). A similar pattern

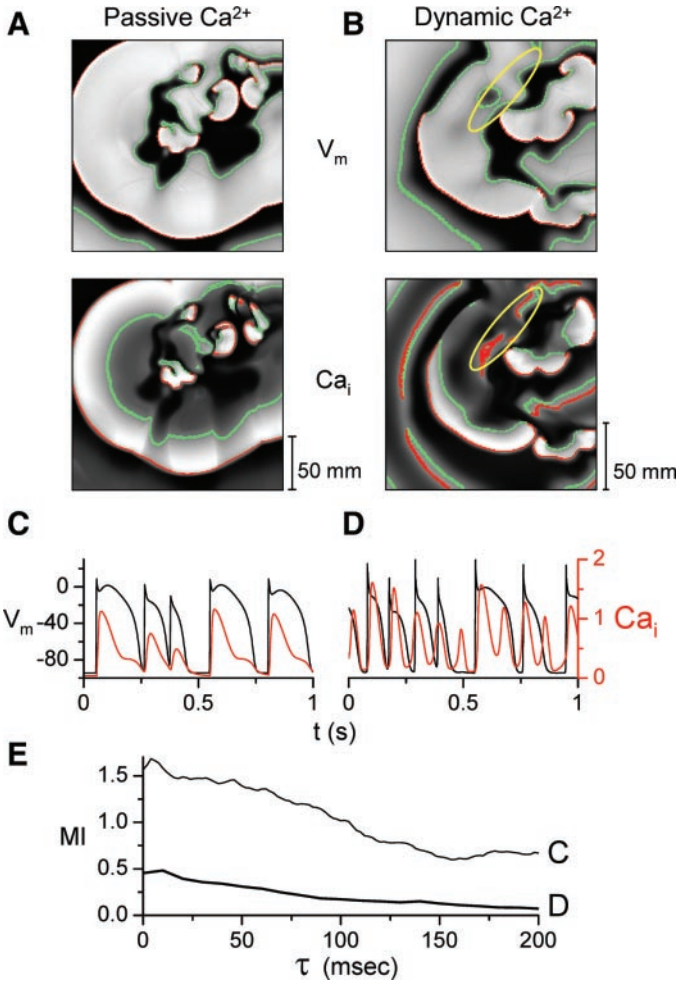


Fig. 4. Two-dimensional tissue simulation of VF using the action potential model with $Ca_i$ passively driven by $V_m$ (passive Ca) or with $Ca_i$ dynamically active in a self-oscillatory mode (dynamic Ca). *A* and *B*: grayscale snapshots of $V_m$ and $Ca_i$ during simulated VF in the two cases. Red lines indicate wavefronts, and green lines indicate wavebacks. The yellow oval in *B* highlights a region in which a rise in $Ca_i$ preceded membrane depolarization, indicating a non-voltage-gated Ca-release event. *C* and *D*: representative superimposed traces of $V_m$ (black lines) and $Ca_i$ (red lines) at a site in the tissue. *E*: MI between $V_m$ and $Ca_i$ as a function of $\tau$ for the $V_m$ and $Ca_i$ traces shown in *C* and *D*, as labeled.

was observed in 15 other reentrant waves during VF in 3 hearts.

Figure 7 compares the spatial dominant frequency (DF) maps of the $V_m$ and Ca signals during 2.3-s recordings of VT in five hearts and VF in five hearts. During VT (Fig. 7*A*), the DFs of the $V_m$ ($DF_{V_m}$) and Ca ($DF_{Ca}$) signals were closely matched over most of the mapped surface, as illustrated best in the difference maps ($DF_{V_m\text{-}Ca}$) obtained by subtracting the DF of the $V_m$ and $Ca_i$ signals at each pixel. In the VT episodes analyzed, the average absolute value of $DF_{V_m\text{-}Ca}$ for all pixels was 1.07 ± 0.66 Hz. In contrast, during VF (Fig. 7*B*), the absolute value of $DF_{V_m\text{-}Ca}$ averaged 5.02 ± 1.22 Hz ($P$ = 0.00022 compared with VT), reflecting that $Ca_i$ was no longer passively tracking $V_m$ alone.

## DISCUSSION

Under normal physiological conditions, regulation of contractile force by $Ca_i$ in the beating heart is tightly controlled by $V_m$, such that the systolic $Ca_i$ transient tracks the AP reliably and consistently with each beat. However, the Ca-induced Ca release system in the heart is an excitable subsystem capable of exhibiting its own dynamics independent of $V_m$, such as propagating $Ca_i$ waves due to regenerative Ca-induced Ca release from the SR in the setting in $Ca_i$ overload (3, 17, 19, 27) and from the endoplasmic reticulum in other tissues (2). In the heart, such $Ca_i$ waves have even been shown to propagate intercellularly from myocyte to myocyte at 0.3–5.5 mm/s (20). Because $Ca_i$ affects $V_m$ via various Ca-sensitive ionic currents, and conversely because $V_m$ affects both Ca-release and Ca-removal processes, these two excitable systems are bidirectionally coupled. This coupling raises the possibility that under pathophysiological conditions, they may destabilize each other sufficiently to influence wavebreak (13). Computer simulations support this scenario. Chudin et al. (4) showed that a stable reentrant spiral wave became destabilized enough to break up into a fibrillation-like state when spontaneous Ca-induced Ca release was allowed to operate in the model.

The purpose of this study was to seek indirect evidence in real cardiac tissue to corroborate this scenario by examining how tightly $Ca_i$ is associated with $V_m$ during VF. We show that the $Ca_i$ transient tracks $V_m$ closely during pacing and VT as

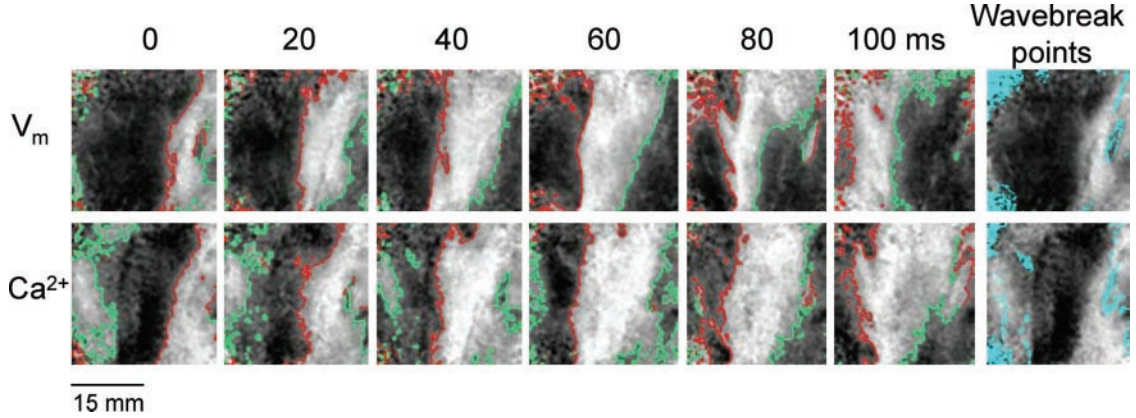


Fig. 5. Snapshots of $V_m$ and $Ca_i$ during VT. For $V_m$ (*top*), the gray scale is black for most hyperpolarized and white for most depolarized, whereas for $Ca_i$ (*bottom*), black is lowest and white is highest. In both cases, red and green lines show wavefront and waveback positions, respectively. The far *right* panel shows all wavebreak points (cyan) during the episode. The $V_m$ wavefront propagates from right to left and is tracked by the $Ca_i$ wavefront with a delay.

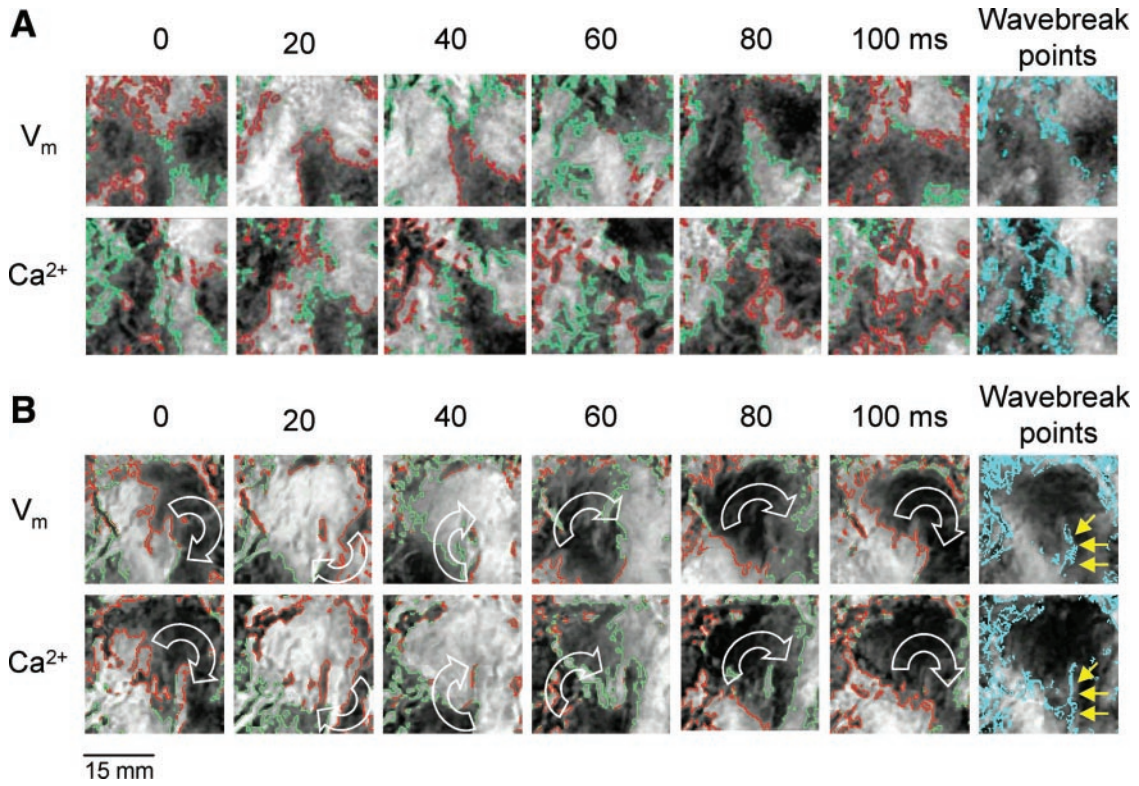


Fig. 6. Snapshots of $V_m$ and $Ca_i$ during VF using the same display format as in Fig. 5. *A*: typical pattern during VF, with multiple $V_m$ waves and a complex distribution of wavebreak points (far *right* panel). The $Ca_i$ wave pattern and wavebreak points bear no consistent relationship to the $V_m$ wave pattern and wavebreak points. *B*: episode of clockwise reentry (white arrows) during VF, which was observed only occasionally and in this example lasted for 7 rotations. The Ca wave tracked (after a delay) the reentrant $V_m$ wave, and the distribution of wavebreak points (yellow arrows) was similar.

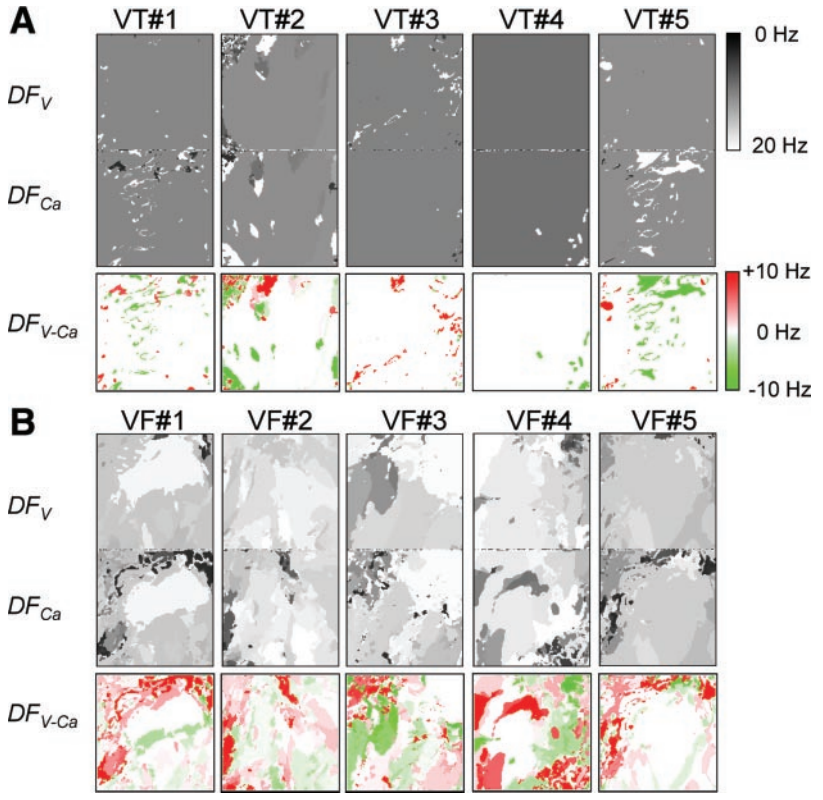


Fig. 7. Spatial distribution of dominant frequency (DF; between 3 and 20 Hz) of optically recorded $V_m$ and $Ca_i$ signals during VT (*A*; 5 episodes) and VF (*B*; 5 episodes). *Top* and *middle*, DF maps of $V_m$ ($DF_V$) and $Ca_i$ ($DF_{Ca}$) on the grayscale indicated; *bottom*, corresponding difference DF maps ($DF_{V\text{-}Ca}$) with red and green representing positive and negative differences, respectively.

expected, but not for the majority of time during VF. During VF, MI between simultaneously recorded traces of $V_m$ and $Ca_i$ was significantly lower than during either pacing or VT. Although MI, which quantifies the extent to which knowledge of one variable's value ($V_m$) predicts the value of a second variable ($Ca_i$), is a statistical measure that does not imply causality, the decreased MI during VF quantitatively indicates that the highly predictable tracking of $Ca_i$ to $V_m$ during pacing and VT is disturbed during VF, as is qualitatively apparent when traces of $V_m$ and $Ca_i$ during VF were superimposed (Fig. 2). A plausible mechanism is that the intrinsic $Ca_i$ dynamics, reflected by non-voltage-gated $Ca_i$-release events, cause $V_m$ and $Ca_i$ to interact in an increasingly less predictable fashion. This conjecture is further was directly supported by simultaneous spatiotemporal maps of $V_m$ and $Ca_i$. These maps showed that when fractionated multiple wavefronts were present during VF, $Ca_i$ waves bore no consistent relationship to membrane depolarization, as they did during pacing and VT. With multiple fractionated wavefronts, $Ca_i$ waves could either precede or follow membrane depolarization, suggesting that both AP-dependent and voltage-independent $Ca_i$ release events were occurring. Only occasionally during VF, when complete reentrant cycles occurred in the mapped area [~15% of the time (25)], did $Ca_i$ waves closely track membrane depolarization (Fig. 6). The analysis of DFs of $V_m$ and $Ca_i$ signals during VF also showed much greater differences during VF than during VT. By virtue of the bidirectional coupling between $Ca_i$ and $V_m$, these observations indicate that $Ca_i$ dynamics influence wave behavior in a complex manner during VF. However, they do not prove that this complex interaction is an independent cause of wavebreak during VF. It is just as possible that increased spatial $Ca_i$ heterogeneity due to non-voltage-gated Ca release could prevent wavebreak as promote it. However, in the computer simulation, the net effect of non-voltage-gated $Ca_i$ release was to increase the incidence of wavebreak.

*Possible mechanisms underlying dissociation of $Ca_i$ and $V_m$ during VF*. The mechanism by which $Ca_i$ is no longer associated with $V_m$ in a consistent and reliable fashion during multiple wavefront VF remains speculative, but several possibilities exist. At a general level, theoretical studies have shown examples in which feedback between two or more coupled excitable systems induces unstable chaotic behavior (7, 14, 21). Wavebreak promoted by Ca-induced Ca release could be an example of this, because the AP and Ca-induced Ca release are coupled excitable systems each capable of exhibiting complex dynamics.

At the cellular level, we speculate that the failure of $Ca_i$ to faithfully track $V_m$ during VF might be explained by spontaneous Ca-induced Ca release becoming dominant over Ca release triggered by the L-type Ca current during the AP. Because Ca transients due to spontaneous Ca-induced Ca release are localized events that propagate only slowly from myocyte to myocyte [0.3–5.5 mm/s (20)], this speculation is consistent with our observation that during VF, $Ca_i$ transients at sites even $<1$ mm apart had a significant drop in MI compared with $Ca_i$ transients during pacing or VT (Fig. 3*C*). $Ca_i$ overload is known to potentiate Ca-induced Ca release and also to predispose hearts to VF. Clusin et al. (5) reported that Ca overload induced VF-like activity in aggregates of cultured chick myocytes, which could be prevented by Ca channel blockers. In intact rabbit hearts in which VF was induced either electrically or by $Ca_i$ overload, Merillat et al. (18) found that Ca channel blockers or removal of extracellular Ca abolished VF. However, ryanodine, which depletes SR Ca (by locking Ca-release channels into an open subconductance state so that the SR becomes leaky) and prevents $Ca_i$ oscillations, did not prevent VF [see also Kusuoka et al. (12)]. Kihara and Morgan (9), using aequorin to record $Ca_i$ directly, found that ryanodine abolished $Ca_i$ oscillations and spontaneous VF, but VF could still be induced electrically. Lappi and Billman (15) also found that spontaneous VF induced by Ca overload was prevented by ryanodine, whereas VF induced by ischemia was not. Saito et al. (23) reported that $Ca_i$ dynamics are the main cause of electrical and mechanical alternans in ventricular muscle, and alternans is well known to predispose the heart to VF (22). In summary, these observations suggest that, although intact $Ca_i$ cycling is not essential for the maintenance of VF in all settings, it exerts a significant profibrillatory effect by enhancing initiation of VF by promoting triggered activity. Our simulations suggest that spatially heterogeneous $Ca_i$ may also promote maintenance of VF by increasing the incidence of wavebreak (13).

Although technical limitations prevented us from measuring absolute changes in resting $Ca_i$ levels in this study, it was shown previously that resting $Ca_i$ can increase significantly to systolic levels during VF, depending on the pharmacological setting (24). This previous study in rat and hamster hearts also documented two types of $Ca_i$ transients during VF, with either minimal (type 1) or preserved (type 2) amplitude modulation. In our experiments in the pig heart, we only observed type 2 $Ca_i$ transients during VF. However, the $Ca_i$ signal in the prior study was spatially averaged over a much larger area (38.5 $mm^2$) than in our study (0.45 $mm^2$), so that the lack of modulation of the $Ca_i$ transient during type 1 VF may have reflected spatial averaging of locally dysynchronous $Ca_i$ signals. This is supported by our observation that $Ca_i$ transients at sites $<1$ mm apart had a significant drop in mutual information compared with pacing or VT (Fig. 3*B*).

*Study limitations*. There are several limitations to this study. The finding that $Ca_i$ is no longer reliably and consistently associated with $V_m$ during VF does not directly address the issue of whether $Ca_i$ dynamics promote or inhibit wavebreak in VF or whether modifying $Ca_i$ dynamics would have antifibrillatory effects. MI is a statistical measure of the relationship between two variables and, if high, indicates an association, but, like all purely statistical measures, does not imply causality. Neither do the simultaneous $V_m$ and $Ca_i$ maps prove that $Ca_i$ cycling promotes or prevents additional wavebreaks during VF. Nevertheless, it is interesting to note that in multiple wavefront VF, regional elevations in $Ca_i$ often preceded membrane depolarization (Fig. 6*A*). This suggests that Ca release was being triggered regionally by non-voltage-gated mechanism(s). In our simulations, the net effect of non-voltage-gated $Ca_i$ release due to dynamically active $Ca_i$ cycling was to increase the incidence of wavebreak, but whether this is also true in real tissue is unproven. Our study also does not shed light into details of the underlying cellular mechanisms: for example, the roles of early or delayed afterdepolarizations, intracellular or intercellular Ca waves, intercellular Ca diffusion, or refractoriness of SR Ca-release channels; the relative importance of specific Ca-sensitive ionic currents that couple $Ca_i$ to $V_m$; or the role of regional tissue heterogeneities in AP

and Ca-release properties that might promote wavebreak under these conditions.

Our studies were conducted at reduced extracellular [Ca] (0.54 mM) but in the absence of excitation-contraction uncouplers such as diacetyl monoxime, raising the possibility that contraction artifacts may have contaminated the optical signals. Even if a motion artifact contaminated the optical $Ca_i$ signal, however, there was still very high MI between $V_m$ and "$Ca_i$." It is difficult to imagine that a contaminating contraction motion would increase MI between the optical $Ca_i$ trace and the microelectrode $V_m$ signal. During VF, contraction (and therefore potential contamination of optical signals by motion) is minimal, yet the MI between $V_m$ and $Ca_i$ decreased compared with pacing or VT. This finding indicates that the calculation of MI is fairly robust and makes it unlikely that the decrease in MI during VF was related to motion artifacts. The reduced extracellular [Ca] would be expected, if anything, to ameliorate $Ca_i$ overload during VF and therefore inhibit the uncoupling of $Ca_i$ from $V_m$. However, MI between $V_m$ and $Ca_i$ still decreased during VF.

Finally, VF was studied in isolated arterially perfused ventricles, whereas VF in in vivo hearts quickly leads to superimposed acute ischemia. Thus our findings are most relevant to the initial phase of VF in the setting of either chronic heart disease or electrically induced VF in the normal heart before acute ischemia sets in. The findings may not apply to VF induced by acute ischemia or other settings (13).

In conclusion, $Ca_i$ is closely associated with $V_m$ closely during pacing and VT but not during the majority of time in VF. The failure of $Ca_i$ to passively track $V_m$ during VF may alter local refractoriness and therefore influence wavefronts affecting the maintenance of VF. Strategies to prevent of VF will need to consider $Ca_i$ cycling dynamics in addition to other factors such as cardiac electrical restitution properties.


## ACKNOWLEDGMENTS

We thank Avile McCullen, Meiling Yuan, and Tan Duong for technical assistance and Elaine Lebowitz for secretarial assistance.

## GRANTS

This study was done during the tenure of a Fellowship Grant from the Cedars-Sinai Electrocardiographic Heartbeat Organization Foundation and Sweepstakes Award (to H. S. Karagueuzian) and was supported in part by National Heart, Lung, and Blood Institute Grants P50HL-52319 and RO1HL-66389, American Heart Association Grants 9750623N, 9950464N, and 025597Y, University of California Tobacco-Related Disease Research Program Grant 11RT-0058, the Ralph M. Parsons Foundation, the Pauline and Harold Price Endowment (to P.-S. Chen), the Laubisch Fund (to J. N. Weiss), and the Kawata Endowment (to J. N. Weiss).


## REFERENCES


1. **Abarbanel HDI.** *Analysis of Observed Chaotic Data*. New York: Springer, 1995.
2. **Berridge MJ.** Elementary and global aspects of calcium signalling. *J Physiol* 499: 291–306, 1997.
3. **Boyden PA, Barbhaiya C, Lee T, and ter Keurs HE.** Nonuniform $Ca^{2+}$ transients in arrhythmogenic Purkinje cells that survive in the infarcted canine heart. *Cardiovasc Res* 57: 681–693, 2003.
4. **Chudin E, Goldhaber J, Garfinkel A, Weiss J, and Kogan B.** Intracellular $Ca^{2+}$ dynamics and the stability of ventricular tachycardia. *Biophys J* 77: 2930–2941, 1999.
5. **Clusin WT, Bristow MR, Karagueuzian HS, Katzung BG, and Schroeder JS.** Do calcium-dependent ionic currents mediate ischemic ventricular fibrillation? *Am J Cardiol* 49: 606–612, 1982.
6. **Efron B and Tibshirani R.** Statistical data analysis in the computer age. *Science* 253: 390–395, 1995.
7. **Endresen LP.** Chaos in weakly-coupled pacemaker cells. *J Theor Biol* 184: 41–50, 1997.
8. **Fox JJ, McHarg JL, and Gilmour RF Jr.** Ionic mechanism of electrical alternans. *Am J Physiol Heart Circ Physiol* 282: H516–H530, 2002.
9. **Kihara Y and Morgan JP.** Intracellular calcium and ventricular fibrillation. Studies in the aequorin-loaded isovolumic ferret heart. *Circ Res* 68: 1378–1389, 1991.
10. **Kim YH, Garfinkel A, Ikeda T, Wu TJ, Athill CA, Weiss JN, Karagueuzian HS, and Chen PS.** Spatiotemporal complexity of ventricular fibrillation revealed by tissue mass reduction in isolated swine ventricle. *J Clin Invest* 100: 2486–2500, 1997.
11. **Kim YH, Xie F, Yashima M, Wu TJ, Valderrabano M, Lee MH, Ohara T, Voroshilovsky O, Doshi RN, Fishbein MC, Qu Z, Garfinkel A, Weiss JN, Karagueuzian HS, and Chen PS.** Role of papillary muscle in the generation and maintenance of reentry during ventricular tachycardia and fibrillation in isolated swine right ventricle. *Circulation* 100: 1450–1459, 1999.
12. **Kusuoka H, Jacobus WE, and Marban E.** Calcium oscillations in digitalis-induced ventricular fibrillation: pathogenetic role and metabolic consequences in isolated ferret hearts. *Circ Res* 62: 609–619, 1988.
13. **Lakatta EG and Guarnieri T.** Spontaneous myocardial calcium oscillations: are they linked to ventricular fibrillation? *J Cardiovasc Electrophysiol* 4: 473–489, 1993.
14. **Landau M and Lorente P.** Conduction block and chaotic dynamics in an asymmetrical model of coupled cardiac cells. *J Theor Biol* 186: 93–105, 1997.
15. **Lappi MD and Billman GE.** Effect of ryanodine on ventricular fibrillation induced by myocardial ischaemia. *Cardiovasc Res* 27: 2152–2159, 1993.
16. **Lee MH, Qu Z, Fishbein GA, Lamp ST, Chang EH, Ohara T, Voroshilovsky O, Kil JR, Hamzei AR, Wang NC, Lin SF, Weiss JN, Garfinkel A, Karagueuzian HS, and Chen PS.** Patterns of wave break during ventricular fibrillation in isolated swine right ventricle. *Am J Physiol Heart Circ Physiol* 281: H253–H265, 2001.
17. **Lipp P and Niggli E.** Microscopic spiral waves reveal positive feedback in subcellular calcium signaling. *Biophys J* 65: 2272–2276, 1993.
18. **Merillat JC, Lakatta EG, Hano O, and Guarnieri T.** Role of calcium and the calcium channel in the initiation and maintenance of ventricular fibrillation. *Circ Res* 67: 1115–1123, 1990.
19. **Miura M, Boyden PA, and ter Keurs HE.** $Ca^{2+}$ waves during triggered propagated contractions in intact trabeculae. *Am J Physiol Heart Circ Physiol* 274: H266–H276, 1998.
20. **Miura M, Boyden PA, and ter Keurs HE.** $Ca^{2+}$ waves during triggered propagated contractions in intact trabeculae. Determinants of the velocity of propagation. *Circ Res* 84: 1459–1468, 1999.
21. **Ostborn P, Wohlfart B, and Ohlen G.** Arrhythmia as a result of poor intercellular coupling in the sinus node: a simulation study. *J Theor Biol* 211: 201–217, 2001.
22. **Pastore JM, Girouard SD, Laurita KR, Akar FG, and Rosenbaum DS.** Mechanism linking T-wave alternans to the genesis of cardiac fibrillation. *Circulation* 99: 1385–1394, 1999.
23. **Saitoh H, Bailey JC, and Surawicz B.** Action potential duration alternans in dog Purkinje and ventricular muscle fibers. Further evidence in support of two different mechanisms. *Circulation* 80: 1421–1431, 1989.
24. **Stefenelli T, Wikman-Coffelt J, Wu ST, and Parmley WW.** Calcium-dependent fluorescence transients during ventricular fibrillation. *Am Heart J* 120: 590–597, 1990.
25. **Valderrabano M, Yang J, Omichi C, Kil J, Lamp ST, Qu Z, Lin SF, Karagueuzian HS, Garfinkel A, Chen PS, and Weiss JN.** Frequency analysis of ventricular fibrillation in Swine ventricles. *Circ Res* 90: 213–222, 2002.
26. **Weiss JN.** Ion channels in cardiac muscle. In: *The Mammalian Myocardium* (2nd ed.), edited by Langer GA. San Diego, CA: Academic, 1997, p. 81–143.
27. **Zhang YM, Miura M, and ter Keurs HE.** Triggered propagated contractions in rat cardiac trabeculae Inhibition by octanol and heptanol. *Circ Res* 79: 1077–1085, 1996.